Experimental Mechanics (2009) 49:719–729
DOI 10.1007/s11340-008-9177-6

An Instrumented Indentation Method for Young's Modulus Measurement with Accuracy Estimation

D. Ma · C.W. Ong · T. Zhang

Received: 22 April 2008 / Accepted: 18 August 2008 / Published online: 23 September 2008

Abstract The relationships between indentation responses and Young's modulus of an indented material were investigated by employing dimensional analysis and finite element method. Three representative tip bluntness geometries were introduced to describe the shape of a real Berkovich indenter. It was demonstrated that for each of these bluntness geometries, a set of approximate indentation relationships correlating the ratio of nominal hardness/reduced Young's modulus H_n/E_r and the ratio of elastic work/total work W_e/W can be derived. Consequently, a method for Young's modulus measurement combined with its accuracy estimation was established on basis of these relationships. The effectiveness of this approach was verified by performing nanoindentation tests on S45C carbon steel and 6061 aluminum alloy and microindentation tests on aluminum single crystal, GCr15 bearing steel and fused silica.

Keywords Young's modulus · Accuracy · Instrumented indentation · Finite element analysis · Berkovich indenter

D. Ma
Department of Mechanical Engineering,
The Academy of Armored Forces Engineering,
Beijing 100072, People's Republic of China

C.W. Ong (✉)
Department of Applied Physics and Materials Research Center,
The Hong Kong Polytechnic University,
Hung Hom, Kowloon, Hong Kong, People's Republic of China
e-mail: apacwong@inet.polyu.edu.hk

T. Zhang
State Key Laboratory of Nonlinear Mechanics (LNM),
Institute of Mechanics, Chinese Academy of Sciences,
Beisihuan West Road 15,
Beijing 100080, People's Republic of China

Introduction

Instrumented indentation has been widely used for determining the mechanical properties of materials on small scales [1–8]. Young's modulus is one of the most commonly concerned material properties determinable with this technique. The pioneer work by Oliver and Pharr [4–6] revealed a famous formula:

$$E_r = \frac{\sqrt{\pi}}{2\beta}\frac{S_u}{\sqrt{A(h_{cm})}} \tag{1}$$

S_u is the initial slope of an unloading curve. E_r is the reduced modulus which is related to the Young's modulus E and Poisson's ratio ν of the indented material and those (E_i, ν_i) of the indenter by the equation $1/E_r = (1-\nu^2)/E + (1-\nu_i^2)/E_i$. β is a constant depending on the shape of the indenter. $A(h_{cm})$ is the projected contact area corresponding to the maximum contact depth h_{cm} when the indenter proceeds to the maximum indentation depth h_m at the maximum load P_m. According to Oliver and Pharr, $A(h_{cm})$ can be directly estimated from the unloading curve. Yet this approach is not always accurate enough. In particular, it does not take account of piling up effect which may occur in the indentation processes of some materials.

Cheng and Cheng presented another fundamental approach [9–11], which was developed for the case when an ideally sharp conical indenter was used. By applying scaling relationships in combination with finite element simulations, they verified the existence of an approximate relationship:

$$H/E_r = f(W_e/W) \tag{2}$$

$H \equiv P_m/A(h_{cm})$ is hardness. W_e and W are the elastic work and total work corresponding to the areas under the unloading and loading curves recorded in an indentation test. By combining equations (1) and (2) to eliminate $A(h_{cm})$, E_r can be determined as:

$$E_r = \left[\pi \Big/ (2\beta)^2\right] f(W_e/W)\left[S_u^2/P_m\right] \tag{3}$$

This formulation gives a first impression that it may be superior to the Oliver and Pharr's model since it does not include h_{cm} [or equivalently $A(h_{cm})$], such that any possible error caused by the uncertainty in deriving h_{cm} from the unloading curve is prevented. However, one should also notice that the model was only usable for the case where an ideally sharp conical indenter is used, so that deviation caused by the bluntness of an indenter tip is not taken into account. Moreover, the quantity S_u is still in the formula, which is needed to be derived from the unloading curve and may carry some error. The error could be large if the data points are scattered, as in the case of a shallow indentation, and in particular, the error is further magnified after taking square as required by equation (3).

In this paper, an improved instrumented indentation method for determining Young's modulus was developed by applying dimensional and finite element analyses. In this method, the bluntness of a non-ideally sharp indenter was considered, and a nominal hardness $H_n=P_m/A(h_m)$ is introduced, which is defined as the maximum load P_m divided by the cross-sectional area $A(h_m)$ evaluated at the maximum indentation depth h_m, and is therefore H_n is fundamentally different from the conventional hardness H. The proposed method can prevent the needs of both the indirectly estimated value of h_{cm} and the quantity of S_u. More importantly, it was developed to be applicable to a broad range of indenter shapes with almost arbitrary tip bluntness and be able to give accuracy estimation on the measurement of Young's modulus.

Theoretical Analysis

Description of Nonideally Sharp Indenters

An indenter with Berkovich geometry is commonly used in a nanoindentation test. A real indenter always has some degree of bluntness, which influence is significant for very shallow indentations. For simplicity, a blunt or non-ideal Berkovich indenter is approximated by a non-ideal conical geometry with a protruding end. The bluntness of the non-ideally sharp indenter was described by introducing two parameters named as volume bluntness ratio V_r and height bluntness ratio h_r. The volume bluntness ratio is defined as $V_r \equiv V_{ideal}/V_{blunt}$, where V_{ideal} is the part of volume bounded by the area $A(h_m)$ for an ideally sharp Berkevich indenter or equivalently conical indenter (Fig. 1), and V_{blunt} is that for a real indenter. The height bluntness ratio is defined as $h_r \equiv h_{ideal}/h_m$, where h_{ideal} is the distance from the vertex of an ideally sharp conical shape to the area $A(h_m)$. Figure 2 shows schematically three tip geometries, which are made to have the same volume bluntness ratio V_r but the respective height bluntness ratios h_r are different. Case 1 refers to a flat-ended geometry, which has the largest value of h_r, and hence is used to represent one extremely blunt situation. Case 2 refers to a conical-tipped geometry with a half-included conical angle α larger than θ=70.3°, namely the half-included angle of a cone giving the same area-to-depth ratio as that of an ideally sharp Berkovich indenter. This geometry is thus regarded to be blunter than the ideal one. Since h_r of this model is the smallest among those of the three models, this geometry is used to represent another extreme situation. The third case is the spherical-capped geometry, which is an intermediate situation between the above two. It can be demonstrated that V_r and h_r are not independent for a specific bluntness type. By using suffixes "f", "c" and "s" to refer to the three typical bluntness geometries, the corresponding relations can be derived, which are $V_r = 1\Big/\left[1-(1-1/h_{rf})^3\right]$ for flat-ended case; $V_r=h_{rc}$ for conical-tipped case; and

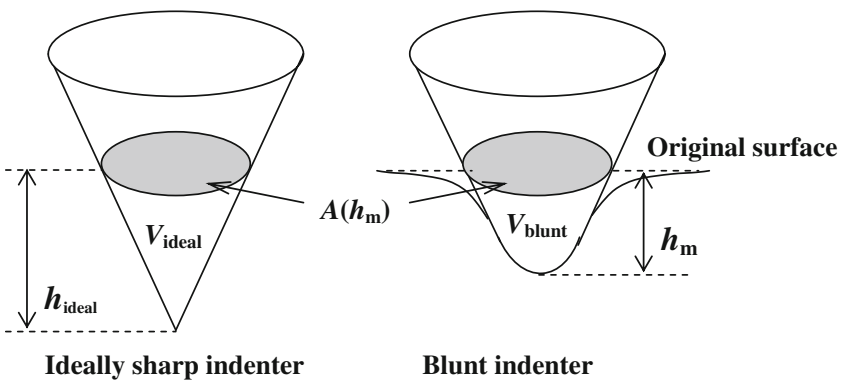

Fig. 1 Schematic diagrams of an ideally sharp indenter and a blunt indenter

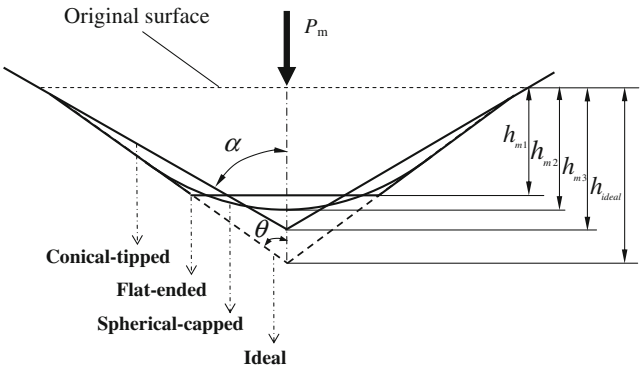

Fig. 2 Three representative blunt geometries and ideally sharp geometry

$V_r = 1\Big/\left[1-(1-1/h_{rs})^3(1+\sin\theta)\right]$ when $V_r \le 1.361$, and $V_r = 2h_{rs}^3\big/\left(3h_{rs}^2+\cot^2\theta\right)$ when $V_r > 1.361$ for spherical-capped case. The condition $V_r=1.361$ specifies a special situation when the maximum indentation depth is equal to the distance between the vertex of the spherical cap and the conical-spherical cap interface. It is noted that a real indenter geometry may not be exactly identical to any one of the three hypothetical models, but is most generally somehow in between. Our presently proposed method of analysis would embrace such a possibility.

Approximate Relationships Between H_n/E_r and W_e/W for Three Types of Non-Ideally Sharp Indenters

Within the framework of continuum mechanics, we apply finite element method to investigate the responses of a material indented by the three representative types of non-ideal conical indenters mentioned above. The indented material is assumed to behave as an isotropic and rate-independent solid, and obeys Von Mises yield criterion and pure isotropic hardening rule. The uniaxial stress–strain relations take the form of linear elasticity combined with the Hollomon's power law hardening, namely:

$$\sigma = \begin{cases} E\varepsilon & ,\varepsilon \le \varepsilon_y \\ \sigma_y\left(\varepsilon/\varepsilon_y\right)^n & ,\varepsilon > \varepsilon_y \end{cases} \tag{4}$$

where σ and ε are the true stress and true strain, and σ_y and $\varepsilon_y=\sigma_y/E$ the yield stress and yield strain. We assume that the indenter is elastic, and no friction exists between the contact interface. The nominal hardness H_n and the work ratio W_e/W are treated as indentation responses, and they should be regarded as functions of the elastoplastic properties (E, ν, σ_y, n) of the tested material, the elastic properties (E_i, ν_i) of the indenter, the maximum indentation depth (h_m), and two bluntness ratios (V_r and h_r). The correlations between these quantities are expressed implicitly as:

$$H_n = f_H\left(E,\nu,\sigma_y,n,E_i,\nu_i,h_m,V_r,h_r\right) \tag{5}$$

$$W_e/W = f_w\left(E,\nu,\sigma_y,n,E_i,\nu_i,h_m,V_r,h_r\right) \tag{6}$$

According to Dao et al. [12] and Fischer–Cripps [13], these two functions may be simplified by introducing the quantity E_r to combine all the elastic effects from the indenter and the indented material, such that equations (5) and (6) can be expressed as:

$$H_n = f_H\left(\sigma_y,n,E_r,h_m,V_r,h_r\right) \tag{7}$$

$$W_e/W = f_w\left(\sigma_y,n,E_r,h_m,V_r,h_r\right) \tag{8}$$

By applying Π theorem of dimensional analysis, functions (7) and (8) can be rewritten in the following dimensionless forms:

$$H_n/E_r = \Phi_H\left(\sigma_y/E_r,n,V_r,h_r\right) \tag{9}$$

$$W_e/W = \Phi_w\left(\sigma_y/E_r,n,V_r,h_r\right) \tag{10}$$

Considering that σ_y/E_r in equation (1) can be expressed in terms of W_e/W, n, V_r and h_r, it can be expressed alternatively as:

$$\sigma_y/E_r = \psi_W\left(W_e/W,n,V_r,h_r\right) \tag{11}$$

By substituting equation (11) into equation (9) to remove σ_y/E_r, the expression of H_n/E_r becomes:

$$H_n/E_r = \Phi_H\left[\psi_W\left(W_e/W,n\right),n,V_r,h_r\right] = \Gamma_H\left(W_e/W,n,V_r,h_r\right) \tag{12}$$

To obtain an explicit result, a commercial finite element code ABAQUS [14] capable of handling large deformation analysis was employed to simulate the non-ideally sharp indentation process. In the calculations, the independent variable σ_y/E_r in equations (9) and (10) was varied in such a way that E_r is kept unchanged by assigning fixed values to E, ν, E_i and ν_i, and let σ_y vary alone. In particular, E_i and ν_i can be removed to get further simplicity by assuming that the indenter is rigid. As such, E and ν are fixed at 70 GPa and 0.3, while σ_y is assigned to vary in a broad range of 0.0005~10.500 GPa. n is assigned by the values of 0, 0.15, 0.3 and 0.45 in sequence, and V_r by 1, 1.336, 2.547 and 4.764. $V_r=1$ refers to the case of ideal tip shape, where $h_r=1$. In a finite element simulation, four-node axisymmetric elements are used. The size of the elements is made to be small enough such that there are at least 30 nodes at the

contact region. The overall dimensions of the model in the radial and axial directions are identical, and the radius of the cross sectional area of the indenter at the maximum indentation depth is constantly below 1/20 of the overall radius of the model. A sensitivity test was performed by looking at the result obtained after reducing the mesh size by one half and doubling the dimensions of the model in both radial and vertical directions. The values of the peak load P_m and the work ratio W_e/W thus obtained do not vary more than 0.5% from those obtained by using the original model, confirming that the original settings of meshing and overall dimension of the model are suitable for simulating a hypothetical indentation made on a semi-infinite solid.

Figure 3 shows some examples of normalized load–unload curves obtained from simulations with the use of the three representative indenter types. Similar simulation processes were performed by assigning some other combinations of σ_y and n, and V_r and h_r. Each set of loading–unloading curves can be used to derive a set of values of H_n/E_r and W_e/W. Figure 4(a)–(c) shows the plots of H_n/E_r versus W_e/W for the flat-ended geometry with V_r=2.547, h_r=6.531, the spherical-capped geometry with V_r=2.547, h_r=3.832 and the conical-tipped geometry with V_r=2.547, h_r=2.547. It is evident from the plots that the data points in each figure fall in a narrow band bounded between the curves with n=0 and 0.45. Therefore, H_n/E_r and W_e/W can be roughly regarded as if they are correlated with a functional relationship, but such a relationship is not perfectly one to one. Similar features can be also observed when an ideally sharp indenter or different degrees of blunt indenters is used.

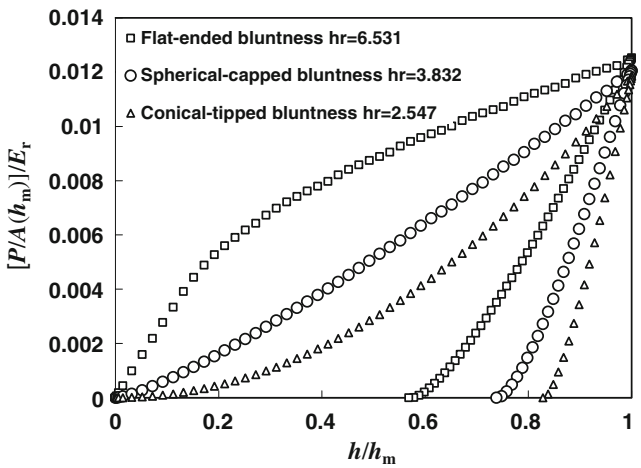

Fig. 3 Normalized load–unload curves obtained from simulations at σ_y=280 MPa, n=0.15, E=70 GPa, ν=0.3 and V_r=2.547, with different h_r's corresponding to the three representative blunt geometries

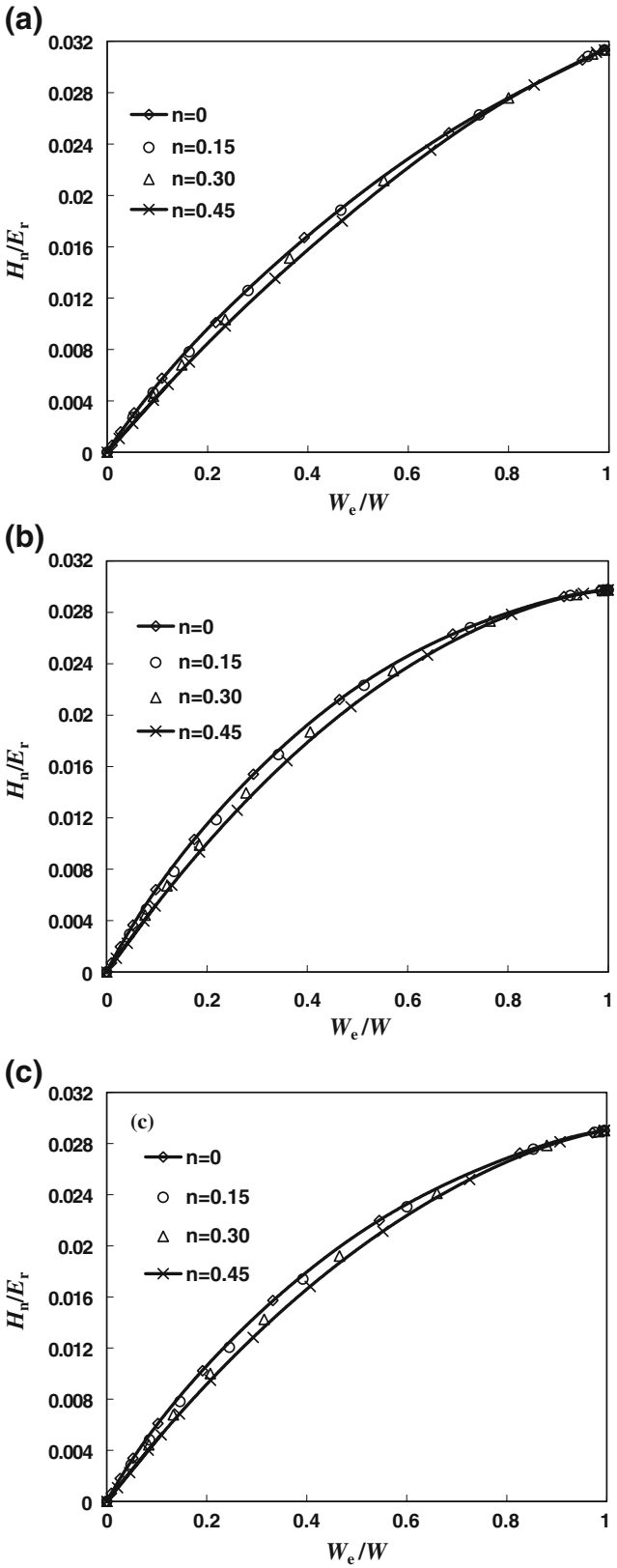

Fig. 4 Relationships between H_n/E_r and W_e/W obtained for (**a**) the flat-ended geometry with V_r=2.547, h_r=6.531, (**b**) the spherical-capped geometry with V_r=2.547, h_r=3.832 and (**c**) the conical-tipped geometry with V_r=2.547, h_r=2.547

Functional Expressions of H_n/E_r–W_e/W Relationships and Accuracy Analysis for Determining E_r

For a certain combination of V_r and h_r, one can create a function $H_n/E_r = F_x(W_e/W)$ to approximate the relationship between H_n/E_r and W_e/W, from which the reduced Young's modulus E_r can be obtained by dividing H_n by H_n/E_r, i.e., $E_r=H_n/(H_n/E_r)=H_n/F_x(W_e/W)$. Obviously, such an estimated E_r would contain some error. The magnitude of the error would depend on how well the simulated H_n/E_r and W_e/W values are fitted to a function. In fact, for a definite value of W_e/W the simulated value (H_n/E_r) varies with n. It is thus reasonable to assign a mean, $\left[1/(H_n/E_r)_{n=0}+1/(H_n/E_r)_{n=0.45}\right]/2$, to represent $1/(H_n/E_r)$ in the analysis. The trend of $left(H_n/E_r)=2/[1/(H_n/E_r)_{n=0}+1/(H_n/E_r)_{n=0.45}]$ with respect to W_e/W can be fitted to a polynomial. We introduce a double-index convention, with the first index "x" to refer to the indenter type, namely, "f", "c" and "s" for flat-ended, conical-tipped and spherical-capped geometries; and the second index "j"=1, 2, 3 and 4 to refer to four selected bluntness levels with volume bluntness ratios $V_{r1}=1$, $V_{r2}=1.336$, $V_{r3}=2.547$ and $V_{r4}=4.764$, respectively. In a compact form, the functions for the three typical indenter types are expressed as:

$$(H_n/E_r)_{xj}=\sum_{i=1}^{6} a_{xi}(V_{rj})(W_e/W)^i \tag{13}$$

Alternatively, in an enumerated format, they are written as:

$$(H_n/E_r)_{fi}=\sum_{i=1}^{6} a_{fi}(V_{ri})(W_e/W)^i \tag{14}$$

$$(H_n/E_r)_{ci}=\sum_{i=1}^{6} a_{ci}(V_{rj})(W_e/W)^i \tag{15}$$

$$(H_n/E_r)_{sj}=\sum_{i=1}^{6} a_{si}(V_{rj})(W_e/W)^i \tag{16}$$

where $a_{fi}(V_{rj})$, $a_{ci}(V_{rj})$ and $a_{si}(V_{rj})$, $(i=1,...,6)$ are the coefficients of the polynomial and their values are given in Table 1.

If $(H_n/E_r)_{xj,n=0}=f_u(W_e/W)$ and $(H_n/E_r)_{xj,n=0.45}=f_l(W_e/W)$ are used to represent the upper and the lower boundaries of an approximate H_n/E_r–W_e/W relationship, the maximum relative errors $|\delta_{rxj}|$ for determining E_r can be calculated from $|\delta_{rxj}|=\left[1/(H_n/E_r)_{xj}-1/(H_n/E_r)_{xj,n=0}\right]/\left[1/(H_n/E_r)_{xj}\right]=1-[\sum_{i=1}^{6} a_{xj}(V_{rj})(W_e/W)^i]/f_u(W_e/W)$ or $|\delta_{rxj}|=\left[1/(H_n/E_r)_{xj,n=0.45}-1/(H_n/E_r)_{xj}\right]/\left[1/(H_n/E_r)_{xj}\right]=[\sum_{i=1}^{6} a_{xj}(V_{rj})(W_e/W)^i]/f_l(W_e/W)-1$. Figure 5 shows the maximum relative error functions of $|\delta_{rfj}|$ $(j=1,2,3,4)$, $|\delta_{rcj}|$ $(j=1,2,3,4)$ and $|\delta_{rsj}|$ $(j=1,2,3,4)$. It is obvious from Fig. 5 that these relative error functions are very close, so that for the convenience of analysis they can be expressed by an average function $|\delta_{br}|$ in a polynomial form of:

$$|\delta_{br}|=\sum_{i=0}^{6} b_i(W_e/W)^i \tag{17}$$

where b_i $(i=0,1,...,6)$ are the coefficients of the polynomial and their values are $b_0=15.67876$, $b_1=-59.77639$, $b_2=102.43439$, $b_3=-58.55967$, $b_4=-69.27250$, $b_5=110.06137$ and $b_6=-40.51260$. As a special case, the maximum relative error function for an ideal Berkovich indenter tip is derived and denoted as $|\delta_r|=|\delta_{rf1}|=|\delta_{rc1}|=|\delta_{rs1}|$, which is slightly smaller than $|\delta_{br}|$, and can be expressed in a polynomial form of:

$$|\delta_r|=|\delta_{rf1}|=|\delta_{rc1}|=|\delta_{rs1}|=\sum_{i=0}^{6} c_i(W_e/W)^i \tag{18}$$

where c_i $(i=0,1,...,6)$ are the coefficients of the polynomial and their values are $c_0=13.29480$, $c_1=-33.35762$, $c_2=6.84133$, $c_3=59.83432$, $c_4=-46.39656$, $c_5=-31.10085$ and $c_6=30.96980$. From Fig. 5 it can be also seen that $|\delta_{br}|$ and $|\delta_r|$ always decrease when the work ratio W_e/W increases. The maximum relative errors derived from equations (17) and (18) at the condition of $W_e/W=0$ are found to be 15.7% for $|\delta_{br}|$, and 13.3% for $|\delta_r|$. Obviously, from the engineering point of view, such a level of accuracy in the measurement of Young's modulus can meet the requirements of most applications.

We note that perfect functional relationship between H_n/E_r and W_e/W for a specific indenter tip is still lacking. It is possible that two materials of different elastoplastic parameters (i.e. E_r, σ_y and n) would give almost identical indentation load–displacement curves and hence the same set of H_n and W_e/W. The estimated E_r value thus derived would deviate from the true values of the respective materials. This is recognized to be the uniqueness problem, which has attracted wide concerns for the measurement of the Young's modulus of an elastoplatic substance with instrumented indentation technique. A systematic study on this problem has been performed recently by Chen et al. [15]. Results of their analysis show that in an indentation cycle with well specified H_n and W_e/W, the ratio of H_n/E_r can vary from the upper bound towards the lower bound of a range when n is set to vary from zero to reach the maximum value specified in their study (it is 0.45 in our study). This finding agrees with the result of our present analysis. In fact, the problem of uniqueness is present in our work, but appears in a form of slight dispersion of E_r due to the uncertainty of n, as reflected by the appearance of a narrow band of H_n/E_r at a specific W_e/W as shown in Fig. 4(a)–(c).

Table 1 The values of coefficients $a_{xi}(V_{rj})$ (x=f, c, s; i=1,...,6; j=1,...,4)

x	j	V_{rj}	$a_{x1}(V_{rj})$	$a_{x2}(V_{rj})$	$a_{x3}(V_{rj})$	$a_{x4}(V_{rj})$	$a_{x5}(V_{rj})$	$a_{x6}(V_{rj})$
f	1	1.000	0.16716	−0.13875	0.06215	0.01568	−0.04784	0.01878
f	2	1.336	0.11088	−0.13538	0.30236	−0.50340	0.41954	−0.13528
f	3	2.547	0.05344	−0.07060	0.18858	−0.31453	0.25048	−0.07588
f	4	4.764	0.02776	−0.03934	0.10015	−0.15016	0.10604	−0.02790
c	1	1.000	0.16716	−0.13875	0.06215	0.01568	−0.04784	0.01878
c	2	1.336	0.12655	−0.14012	0.20772	−0.29096	0.22433	−0.07001
c	3	2.547	0.06482	−0.07744	0.14161	−0.22246	0.18104	−0.05782
c	4	4.764	0.03393	−0.04164	0.08170	−0.13158	0.10712	−0.03376
s	1	1.000	0.16716	−0.13875	0.06215	0.01568	−0.04784	0.01878
s	2	1.336	0.11612	−0.14391	0.29892	−0.50592	0.43731	−0.14669
s	3	2.547	0.05899	−0.06815	0.13162	−0.21203	0.17552	−0.05691
s	4	4.764	0.03104	−0.03438	0.06404	−0.10089	0.08154	−0.02588

The stability for the determination of E_r can be examined by investigating the sensitivity of E_r with respect to perturbations of H_n and W_e/W. For all of the three indenter geometries and four bluntness levels specified in this work, the dispersion of E_r calculated from the formula $E_r = H_n \Big/ (H_n/E_r)_{xj} = H_n \Big/ \left[\sum_{i=1}^{6} a_{xi}(V_{rj})(W_e/W)^i\right]$ by varying W_e/W with ±5% around a centered value selected arbitrarily from a range of 0.01~1 is less than ∓5.2%, while the same change of H_n would lead to the same variation of E_r. It is thus concluded that E_r exhibits a rather good stability over small perturbations of H_n and W_e/W.

Proposed Method

The establishment of equations (13), (17) and (18) forms the basis for Young's modulus measurement and its accuracy estimation. For a nanoindentation test, the procedures proposed for the purpose are listed in detail as follows:

(i) Calibrate the area function $A(h)$ of a real Berkovich indenter used for indentation tests according to the tip calibration procedures proposed by Oliver and Pharr [4, 6].

(ii) Generate loading and unloading curves by performing indentations on the tested material with a depth-sensing indentation system. P_m and h_m are directly measured, and $A(h_m)$ is derived from the area function obtained in step (i). Hence, the value of the nominal hardness $H_n \equiv P_m/A(h_m)$ is determined. Further, the work ratio W_e/W is determined, where W_e and W are obtained by integrating the areas under the unloading and loading curves, respectively.

(iii) Calculate the volume bluntness ratio $V_r \equiv V_{ideal}/V_{blunt}$, where $V_{ideal} = (1/3)A(h_m)[A(h_m)/24.5]^{0.5}$ for an ideal Berkovich indenter, and $V_{blunt} = \int_0^{h_m} A(h)\,dh$ for the real Berkovich indenter.

(iv) Calculate the height bluntness ratio $h_r \equiv h_{ideal}/h_m$ for the real Berkovich indenter, where $h_{ideal} = [A(h_m)/24.5]^{0.5}$. Then, calculate the height bluntness ratios h_{rf}, h_{rc} and h_{rs} associated with the three typical types of blunt tips by substituting the V_r value obtained in (iii) into the expressions relating the two bluntness ratios given in "Theoretical Analysis".

(v) Write down the Expressions (14–16) with the coefficients tabulated in Table 1 for the three typical tip shapes and four different levels of bluntness specified by V_{rj}=1, 1.336, 2.547 and 4.764 indexed with j=1,...,4. Then substitute W_e/W into the formulas to calculate the values of $(H_n/E_r)_{fj}$, $(H_n/E_r)_{cj}$ and $(H_n/E_r)_{sj}$.

(vi) Derive the best fit to the four data points of $(H_n/E_r)_{fj}$ versus V_{rj} (j=1,2,3,4) by using a third-order polynomial of $1/V_{rj}$. A best estimate of $(H_n/E_r)_f$ corresponding to V_r obtained in (iii) is thus derived

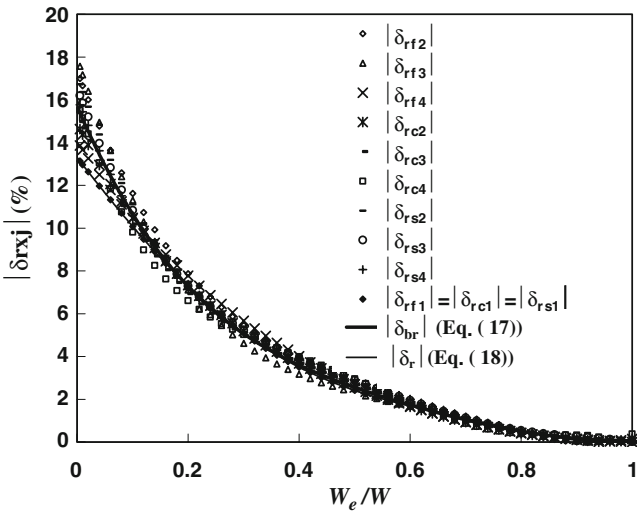

Fig. 5 Relative error functions $|\delta_{rxj}|$ (x=f, c, s; j=1,2,3,4) and $|\delta_{br}|$

via interpolation. The best estimates of $(H_n/E_r)_c$ and $(H_n/E_r)_s$ are obtained with the same technique.

(vii) Derive the best fit to the data points of $(H_n/E_r)_x$ versus h_{rx} (x=f, c, s) by using a second-order polynomial of h_r. Based on this relationship, a best estimate of H_n/E_r at V_r and h_r is derived by interpolation.

(viii) Determine the reduced Young's modulus $E_r=H_n/(H_n/E_r)$, and the maximum relative error $|\delta_{br}|$ of E_r by applying equation (17). Then calculate the maximum Young's modulus E_{max} and the minimum Young's modulus E_{min} of the tested material by using the expressions $E_{max}=(1-\nu^2)/\{1/[E_r(1+|\delta_{br}|)]-(1-\nu_i^2)/E_i\}$ and $E_{min}=(1-\nu^2)/\{1/[E_r(1-|\delta_{br}|)]-(1-\nu_i^2)/E_i\}$ respectively, provided that the values of E_i, ν_i and ν are all known. Finally determine the average Young's modulus $E=(E_{max}+E_{min})/2$, and its maximum relative error $|\delta_b|=(E_{max}-E)/E=-(E_{min}-E)/E=|\delta_{br}|\Big/\left[1-\left(1-|\delta_{br}|^2\right)(1-\nu_i^2)E_r/E_i\right]$.

For a microindentation test, both the values of the two indenter bluntness parameters of V_r and h_r are close to 1. Therefore, the influence of the indenter tip bluntness on the ratio of H_n/E_r can be neglected. The values of H_n/E_r and E_r can be directly estimated from the 6 equations $H_n/E_r=(H_n/E_r)_{f1}=(H_n/E_r)_{c1}=(H_n/E_r)_{s1}=\sum_{i=1}^{6}a_{fi}(V_{r1})(W_e/W)^i=\sum_{i=1}^{6}a_{ci}(V_{r1})(W_e/W)^i=\sum_{i=1}^{6}a_{si}(V_{r1})(W_e/W)^i$ and $E_r=H_n/\left(H_n/E_r\right)$ respectively. The value of $|\delta_r|$ can be determined by $|\delta_r|=|\delta_{rf1}|=|\delta_{rc1}|=|\delta_{rs1}|=\sum_{i=0}^{6}c_i(W_e/W)^i$. Consequently, the Young's modulus E of the tested material and its maximum relative error $|\delta|$ can be determined as $E=(E_{max}+E_{min})/2=0.5(1-\nu^2)/\{1/[E_r(1+|\delta_r|)]-(1-\nu_i^2)/E_i\}+0.5(1-\nu^2)/\{1/[E_r(1-|\delta_r|)]-(1-\nu_i^2)/E_i\}$ and $|\delta|=(E_{max}-E)/E=-(E_{min}-E)/E=|\delta_r|\Big/\left[1-\left(1-|\delta_r|^2\right)(1-\nu_i^2)E_r/E_i\right]$, respectively.

Experiments

Nanoindentation Tests

In this subsection, we use the proposed method to analyze the data of shallow indentations, where the indenter tip bluntness effect is not negligible. Two materials, i.e. S45C carbon steel and 6061 aluminum alloy, were selected for investigations. Each specimen of the two materials was polished to produce mirror-reflecting surfaces for indentation tests. The polishing processes were performed by using grinding papers of 800, 1,200, 2,000 and 4,000 grits, and then diamond pastes of 6, 3, 1 and 0.25 μm grain sizes. Atomic force microscopy analysis showed that the root mean square roughness of the polished surface was around 0.5 nm in a detected surface of 15 μm^2. To obtain references of the E values, uniaxial tensile tests for the two selected materials were performed. Results for the S45C carbon steel and 6061 aluminum alloy are found to be 200.1 and 70.5 GPa, respectively.

A commercial Nano Indenter® XP equipped with a Berkovich indenter was used for the measurements. The area function $A(h)$ of the indenter was derived according to Oliver and Pharr's procedures [4, 6]. Indentation tests with full loads of 0.315 and 0.312 mN were performed on a carbon steel specimen and a 6061 aluminum alloy specimen. Each indentation test consisted of an approaching segment, a loading segment, a holding segment, an unloading segment and a thermal drift correction segment. Five repetitive measurements were conducted at different positions on a sample surface in order to give an average result. Typical load–unload curves for S45C carbon steel and 6061 aluminum alloy are shown in Figs. 6 and 7. Influences due to thermal drift and load frame stiffness were diminished through standard correction procedures. We refer to the experimental curve shown in Fig. 6 as an example to demonstrate the process to derive E and $|\delta_b|$. The main results are listed in Table 2. In the analysis, E_i and ν_i are set to be 1,141 GPa and 0.07; and the values of ν of carbon steel and aluminum alloy were assigned to be 0.3 and 0.33, respectively.

The procedures for analyzing the indentation data of S45C carbon steel and 6061 aluminum alloy are identical. Results obtained from all measurements are shown in Table 3. It can be seen that both the average values of E of the two materials determined with the present method are close to the reference values. The relative errors are 10.7% for S45C carbon steel and 5.6% for 6061 aluminum alloy, respectively, and are all smaller than their theoretical maximum values of 11.3% and 8.0%. This indicates

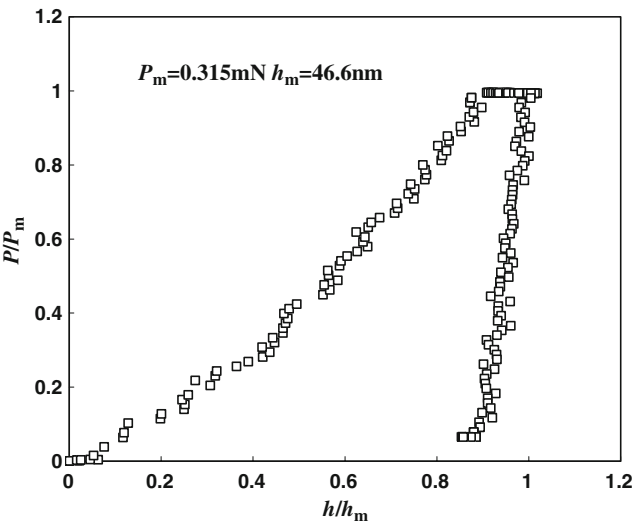

Fig. 6 Typical nanoindentation load–displacement curves for S45C carbon steel

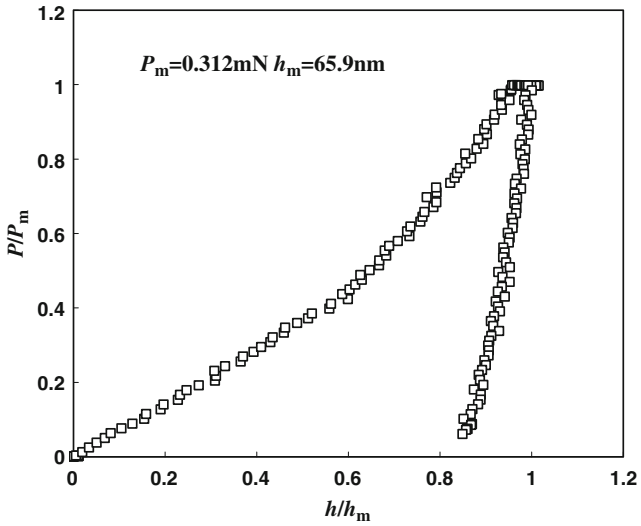

Fig. 7 Typical nanoindentation load–displacement curves for 6061 aluminum alloy

that the present method is effective for nanoindentation tests. In addition, the relative error of 10.7% for S45C carbon steel is found to be larger than that of 5.6% for 6061 aluminum alloy. This is explained because the predicted maximum relative error of the estimated E_r, namely $|\delta_{br}|$ and that of the estimated E, namely $|\delta_b| = |\delta_{br}| \Big/ \left[1 - \left(1 - |\delta_{br}|^2\right)\left(1 - \nu_i^2\right)E_r/E_i\right]$ would increase with decreasing work ratio W_e/W (Fig. 5). Since S45C carbon steel has a smaller work ratio W_e/W than that of 6061 aluminum alloy, the former is therefore expected to have larger relative error of the estimated E_r and E.

For comparison, the results of Young's moduli $E_{O\&P}$ determined by the Oliver & Pharr method are also shown in Table 3. It is obvious that for a material like S45C carbon steel with a moderate strain hardening exponent of about 0.15, the traditional method may provide a good estimate on the Young's modulus, while for a material like 6061 aluminum alloy with a small strain hardening exponent of

Table 2 Main results obtained from test 1 on S45C carbon steel

Steps	Main results
(i)	$A(h) = 26.2644h^2 + 1,255.2840h - 1,951.4068h^{1/2} - 61.7471h^{1/4} + 945.9002h^{1/8}$ P_m=0.315 mN, h_m=46.6 nm, $H_n \equiv P_m/A(h_m) = 3.02$ GPa,, W_e/W=0.126
(ii)	$V_r \equiv V_{ideal}/V_{blunt} = (1/3)A(h_m)[A(h_m)/24.5]^{0.5} \Big/ \int_0^{h_m} A(h)\,dh = 1.186$
(iii)	$h_r \equiv h_{ideal}/h_m = [A(h_m)/24.5]^{0.5} \Big/ h_m = 1.395$, $h_{rf} = 1 \Big/ \left[1 - (1 - 1/V_r)^{1/3}\right] = 2.172$, $h_{rc} = V_r = 1.186$, $h_{rs} = 1/\left\{1 - \left[(1 - 1/V_r)/(1 + \sin\theta)\right]^{1/3}\right\} = 1.762$
(iv)	$(H_n/E_r)_{fj} = \sum_{i=1}^{6}\left[a_{fi}(V_{rj})\right](W_e/W)^i = 0.0190, 0.0123, 0.0059, 0.0030$ for $j = 1,2,3,4$ $(H_n/E_r)_{cj} = \sum_{i=1}^{6}\left[a_{ci}(V_{rj})\right](W_e/W)^i = 0.0190, 0.0141, 0.0072, 0.0037$ for $j = 1,2,3,4$ $(H_n/E_r)_{sj} = \sum_{i=1}^{6}\left[a_{si}(V_{rj})\right](W_e/W)^i = 0.0190, 0.0128, 0.0066, 0.0035$ for $j = 1,2,3,4$
(v)	$(H_n/E_r)_f = \sum_{k=1}^{4}\left[(H_n/E_r)_{fk}\prod_{\substack{j=1\\ j\neq k}}^{4}\left(1/V_r - 1/V_{rj}\right)/\left(1/V_{rk} - 1/V_{rj}\right)\right] = 0.0145$ $(H_n/E_r)_c = \sum_{k=1}^{4}\left[(H_n/E_r)_{ck}\prod_{\substack{j=1\\ j\neq k}}^{4}\left(1/V_r - 1/V_{rj}\right)/\left(1/V_{rk} - 1/V_{rj}\right)\right] = 0.0159$ $(H_n/E_r)_s = \sum_{k=1}^{4}\left[(H_n/E_r)_{sk}\prod_{\substack{j=1\\ j\neq k}}^{4}\left(1/V_r - 1/V_{rj}\right)/\left(1/V_{rk} - 1/V_{rj}\right)\right] = 0.0149$
(vi)	$H_n/E_r = (H_n/E_r)_f\{(h_r - h_{rc})(h_r - h_{rs})/(h_{rf} - h_{rc})(h_{rf} - h_{rs})\}$ $+ (H_n/E_r)_c\{(h_r - h_{rf})(h_r - h_{rs})/(h_{rc} - h_{rf})(h_{rc} - h_{rs})\}$ $+(H_n/E_r)_s\{(h_r - h_{rf})(h_r - h_{rc})/(h_{rs} - h_{rf})(h_{rs} - h_{rc})\} = 0.0155$
(vii)	$E_r = H_n/(H_n/E_r) = 196.5$ GPa $\lvert\delta_{br}\rvert = \sum_{i=0}^{6} b_i(W_e/W)^i = 9.6\%$
(viii)	$E_{max} = (1 - \nu^2)/\left\{1/[E_r(1 + \lvert\delta_{br}\rvert)] - \left(1 - \nu_i^2\right)/E_i\right\} = 241.1$ GPa $E_{min} = (1 - \nu^2)/\left\{1/[E_r(1 - \lvert\delta_{br}\rvert)] - \left(1 - \nu_i^2\right)/E_i\right\} = 191.2$ GPa $E = (E_{max} + E_{min})/2 = 216.3$ GPa $\lvert\delta_b\rvert = (E_{max} - E)/E = -(E_{min} - E)/E = 11.6\%$

Table 3 The values of E_r, E, $|\delta_{br}|$ and $|\delta_b|$ for S45C carbon steel and 6061 aluminum alloy determined from the present method and Oliver & Pharr method combined with nanoindentation tests

	h_m (nm)	h_r	V_r	W_e/W	H_n (GPa)	H_n/E_r	E_r (GPa)	$\pm\|\delta_{br}\|$ (%)	E (GPa)	$\pm\|\delta_b\|$ (%)		$E_{O\&P}$ (GPa)	
(a) S45C carbon steel											$(E-200.1)/E$		$(E_{O\&P}-200.1)/E_{O\&P}$
Test 1	46.6	1.395	1.186	0.126	3.041	0.0155	196.5	±9.6	216.3	±11.6	7.5%	197.6	−1.3%
Test 2	45.7	1.401	1.190	0.128	3.138	0.0156	201.2	±9.6	222.6	±11.6	10.1%	211.2	5.3%
Test 3	45.2	1.404	1.192	0.129	3.193	0.0157	203.4	±9.5	225.5	±11.6	11.3%	202.7	1.3%
Test 4	40.6	1.435	1.212	0.170	3.787	0.0196	193.2	±8.1	211.8	±9.8	5.5%	206.1	2.9%
Test 5	43.5	1.415	1.199	0.128	3.395	0.0155	219.0	±9.6	247.0	±11.8	19.0%	256.9	22.1%
Average									224.6	±11.3	10.7%	214.9	6.9%
(b) 6061 aluminum alloy											$(E-70.5)/E$		$(E_{O\&P}-70.5)/E_{O\&P}$
Test 1	64.6	1.314	1.138	0.191	1.768	0.0234	75.6	±7.5	72.2	±8.1	2.3%	76.3	7.6%
Test 2	60.1	1.330	1.147	0.223	1.992	0.0263	75.7	±6.7	72.2	±7.1	2.4%	77.4	8.9%
Test 3	64.8	1.313	1.137	0.202	1.759	0.0245	71.8	±7.2	68.3	±7.7	−3.3%	80.5	12.4%
Test 4	62.1	1.323	1.143	0.184	1.888	0.0225	83.9	±7.7	80.7	±8.3	12.6%	91.4	22.9%
Test 5	65.9	1.309	1.135	0.164	1.711	0.0206	83.1	±8.3	79.9	±9.0	11.7%	93.1	24.3%
Average									74.7	±8.0	5.6%	83.7	15.8%

about 0.04, the currently proposed method appears to be more effective than the traditional one. It is thus further inferred that the relatively low strain hardening exponent of 6061 aluminum alloy would cause pile-up effect, which is supposed to be the main reason responsible for the lower accuracy in estimating the Young's modulus of the material by applying the Oliver & Pharr method.

Microindentation Tests

In this subsection, three materials, i.e. aluminum single crystal, GCr15 bearing steel and fused silica were selected for investigations, where the aluminum single crystal and fused silica are standard samples provided by MTS. Their reference Young's modulus values as claimed by MTS are 70.4 and 72 GPa, respectively. The reference value for GCr15 bearing steel is determined to be 204 GPa by applying standard ultrasonic measurement. Another Nano Indenter® XP equipped with a Berkovich indenter was used to perform microindentation tests. The area function $A(h)$ of the indenter was calibrated as $A(h)=24.4974h^2+424.149h+2{,}8211.4h^{1/2}-6{,}9751.1h^{1/4}-46{,}333.3h^{1/8}-7{,}055.7h^{1/16}+20{,}987.7h^{1/32}+37{,}312.2h^{1/64}+46{,}075.9h^{1/128}$. An experiment was repeated five times to obtain five sets of load–displacement curves as shown in Figs. 8, 9 and 10. The Poisson's ratio ν of aluminum single crystal, GCr15 bearing

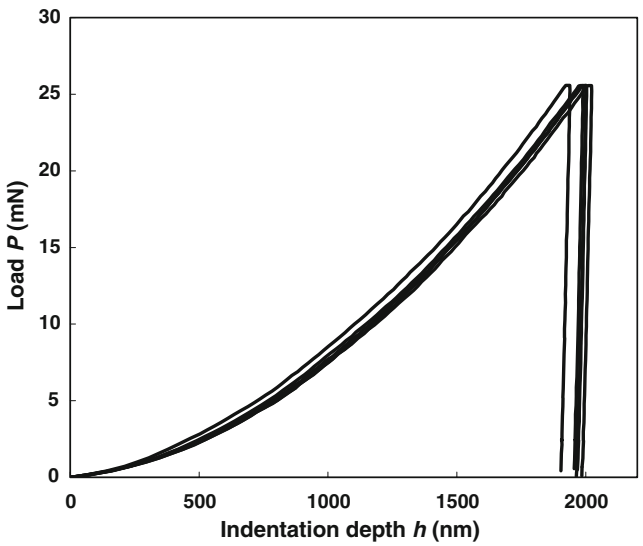

Fig. 8 Load–displacement curves of five repetitive tests made on aluminum single crystal

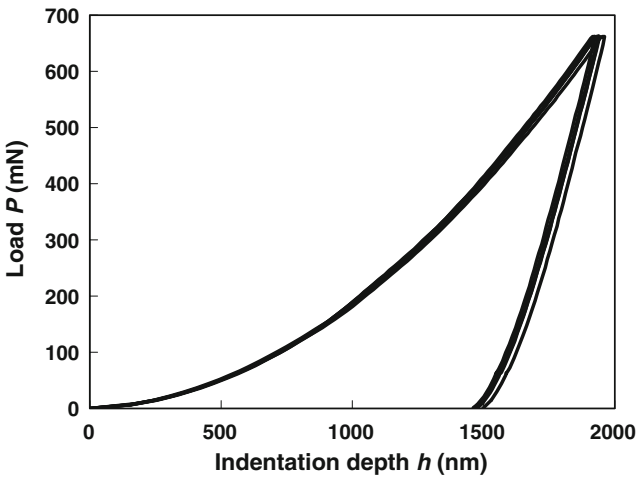

Fig. 9 Load–displacement curves of five repetitive tests made on GCr15 bearing steel

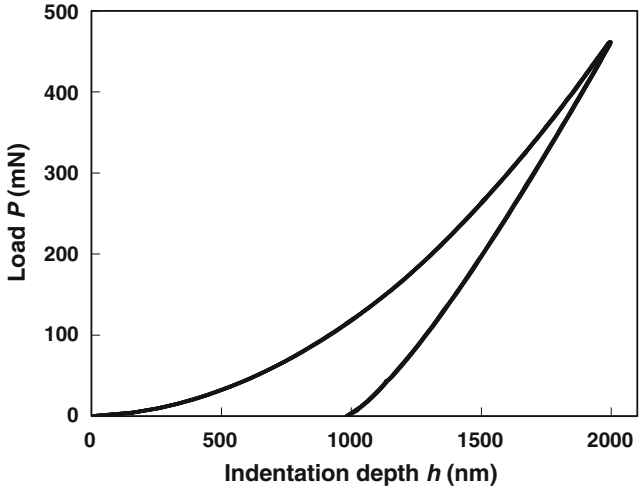

Fig. 10 Load–displacement curves of five repetitive tests made on fused silica

steel and fused silica were assigned to be 0.347, 0.3 and 0.17, respectively. By applying the proposed method, the Young's modulus E of the three tested materials and their maximum relative error $|\delta|$ were determined, and the results are given in Table 4. It is seen that the estimated values of Young's modulus of GCr15 bearing steel and fused silica are very close to the reference values, while that of aluminum single crystal shows a little large deviation from its reference value. This validates the theoretic prediction once again that the maximum error of an estimated E should increase with decreasing work ratio W_e/W. In addition, all the relative errors (average) of the estimated E for the three materials are smaller than their theoretical maximum values of $|\delta|$, indicating that the presented method is also effective for microindentation tests. Also shown in Table 4 are the results of Young's moduli $E_{O\&P}$ determined by the Oliver & Pharr method. It is evident that the presently proposed method is more accurate in measuring Young's modulus than the traditional one.

Conclusions

In this paper, dimensional analysis and finite element simulations were employed to investigate a set of approximate relationships between H_n/E_r and W_e/W for different types of Berkovich tip geometries with different degree of bluntness. These relationships were found to be not perfectly one to one due to the uncertainty of strain hardening exponent n. Through creating a set of functions of $(H_n/E_r)_{xj} = \sum_{i=1}^{6} a_{xi}(V_{rj})(W_e/W)^i$ (x=f, c, s; j=1,2,3,4) for various typical indenter geometries and different degrees of

Table 4 The values of E_r, E, $|\delta_r|$ and $|\delta|$ for aluminum single crystal, GCr15 bearing steel and fused silica determined from the present method and Oliver & Pharr method combined with microindentation tests

	h_m (nm)	h_r	V_r	W_e/W	H_n (GPa)	H_n/E_r	E_r (GPa)	$\pm\lvert\delta_r\rvert$ (%)	E (GPa)	$\pm\lvert\delta\rvert$ (%)		$E_{O\&P}$(GPa)	
(a) Aluminum single crystal											$(E-70.4)/E$		$(E_{O\&P}-70.4)/E_{O\&P}$
Test 1	2,000.7	1.008	0.998	0.0262	0.256	0.00429	59.6	±12.4	55.4	±13.1	−27.1%	69.8	−0.9%
Test 2	2,003.6	1.008	0.998	0.0193	0.255	0.00318	80.2	±12.7	76.0	±13.6	7.3%	62.7	−12.3%
Test 3	1,990.0	1.008	0.998	0.0259	0.259	0.00424	61.0	±12.4	56.8	±13.1	−24.0%	66.2	−6.3%
Test 4	2,023.1	1.008	0.998	0.0219	0.250	0.00359	69.6	±12.6	65.3	±13.4	−7.9%	56.4	−24.8%
Test 5	1,938.4	1.009	0.998	0.0205	0.272	0.00337	80.8	±12.6	76.6	±13.6	8.1%	68.8	−2.3%
Average									66.0	±13.3	−6.7%	64.8	−8.6%
(b) GCr15 bearing steel											$(E-204)/E$		$(E_{O\&P}-204)/E_{O\&P}$
Test 1	1,923.7	1.009	0.998	0.288	7.156	0.0382	187.5	±5.3	204.1	±6.4	0.1%	218.5	6.6%
Test 2	1,941.5	1.009	0.998	0.288	7.026	0.0382	184.0	±5.3	199.6	±6.3	−2.2%	212.1	3.8%
Test 3	1,938.5	1.009	0.998	0.282	7.048	0.0375	187.9	±5.4	204.7	±6.5	0.3%	215.2	5.2%
Test 4	1,962.3	1.008	0.998	0.283	6.880	0.0376	183.1	±5.4	198.4	±6.5	−2.8%	213.6	4.5%
Test 5	1,936.4	1.009	0.998	0.288	7.063	0.0381	185.2	±5.3	201.1	±6.3	−1.4%	216.5	5.8%
Average									201.6	±6.4	−1.2%	215.2	5.2%
(c) Fused silica											$(E-72)/E$		$(E_{O\&P}-72)/E_{O\&P}$
Test 1	1,996.8	1.008	0.998	0.667	4.632	0.0666	69.5	±1.3	71.9	±1.4	−0.2%	71.5	−0.7%
Test 2	1,998.8	1.008	0.998	0.664	4.623	0.0665	69.5	±1.3	71.9	±1.4	−0.1%	71.8	−0.3%
Test 3	1,996.7	1.008	0.998	0.664	4.633	0.0665	69.7	±1.3	72.1	±1.4	0.1%	72.0	0.0%
Test 4	1,996.2	1.008	0.998	0.661	4.635	0.0664	69.9	±1.3	72.2	±1.4	0.3%	72.2	0.3%
Test 5	1,996.4	1.008	0.998	0.666	4.634	0.0666	69.6	±1.3	71.9	±1.4	−0.1%	72.6	0.8%
Average									72.0	±1.4	0.0%	72.0	0.0%

bluntness, the reduced Young's modulus E_r and its maximum relative error $|\delta_{rxj}|$ (x=f, c, s; j=1,2,3,4) can be deduced. It was found from the present analysis that the maximum relative error $|\delta_{rxj}|$ of the estimated E_r for the three indenter geometries and four bluntness levels are very close, and can be thus expressed by a unified average error $|\delta_{br}|$. As a special case, the relative error $|\delta_r| = |\delta_{rf1}| = |\delta_{rc1}| = |\delta_{rs1}|$ of the estimated E_r with an ideal Berkovich indenter tip has a slightly smaller value than $|\delta_{br}|$. In particular, the values of $|\delta_{br}|$ and $|\delta_r|$ always decrease with increasing work ratio W_e/W, and the maximum values are found to be 15.7% for $|\delta_{br}|$ and 13.3% for $|\delta_r|$ at W_e/W=0. Based on the establishment of functions $(H_n/E_r)_{xj}$ (x=f, c, s; j=1,2,3,4), $|\delta_{br}|$ and $|\delta_r|$, a general methodology for determining Young's modulus E and its maximum relative error $|\delta_b|$ or $|\delta|$ was proposed.

The presented method was examined by nanoindentation tests performed on S45C carbon steel and 6061 aluminum alloy, and microindentation tests on aluminum single crystal, GCr15 bearing steel and fused silica. Experimental results showed that the proposed method for determining Young's modulus and its maximum relative error is effective.

Acknowledgment This work was supported by the National Natural Science Foundation of China (Grant No. 10672185).

References

1. Pethicai JB, Hutchings R, Oliver WC (1983) Hardness measurement at penetration depth as small as 20 nm. Philos Mag A 48:593–606. doi:10.1080/01418618308234914.
2. Loubet JL, Georges JM, Marchesini O, Meille G (1984) Vickers indentation curves of magnesium oxide (MgO). J Tribol 106:43–48.
3. Newey D, Wilkens MA, Pollock HM (1982) An ultra-low-load penetration hardness tester. J Phys E 15:119–122. doi:10.1088/0022-3735/15/1/023.
4. Oliver WC, Pharr GM (1992) An improved technique for determining hardness and elastic modulus using load and displacement sensing indentation experiments. J Mater Res 7:1564–1583. doi:10.1557/JMR.1992.1564.
5. Pharr GM, Oliver WC, Brotzen FR (1992) On the generality of the relationship among contact stiffness, contact area, and elastic modulus during indentation. J Mater Res 7:613–617. doi:10.1557/JMR.1992.0613.
6. Oliver WC, Pharr GM (2004) Measurement of hardness and elastic modulus by instrumented indentation: advances in understanding and refinements to methodology. J Mater Res 19:3–20. doi:10.1557/jmr.2004.19.1.3.
7. Cheng Y-T, Cheng CM (2004) Scaling, dimension analysis, and indentation measurements. Mater Sci Eng R Rep 44:91–149. doi:10.1016/j.mser.2004.05.001.
8. Fischer-Cripps AC (2004) Nanoindentation. Springer, New York, p 39.
9. Cheng Y-T, Cheng CM (1998) Relationships between hardness, elastic modulus, and the work of indentation. Appl Phys Lett 73:614–616. doi:10.1063/1.121873.
10. Cheng CM, Cheng Y-T (1997) On the initial unloading slope in indentation of elastic-plastic solids by an indenter with an axisymmetric smooth profile. Appl Phys Lett 71:2623–2625. doi:10.1063/1.120159.
11. Ni WY, Cheng Y-T, Cheng CM, Grummon DS (2004) An energy-based method for analyzing instrumented spherical indentation experiments. J Mater Res 19:149–157. doi:10.1557/jmr.2004.19.1.149.
12. Dao M, Chollacoop N, Van Vliet KJ, Venkatesh TA, Suresh S (2001) Computational modeling of the forward and reverse problems in instrumented sharp indentation. Acta Mater 49:3899–3918. doi:10.1016/S1359-6454(01)00295-6.
13. Fischer-Cripps AC (2003) Use of combined elastic modulus in depth-sensing indentation with a conical indenter. J Mater Res 18:1043–1045. doi:10.1557/JMR.2003.0144.
14. Hibbitt, Karlsson & Sorensen, Inc. (2001) *ABAQUS/Standard 6.2 User's Manual*
15. Chen X, Ogasawara N, Zhao M, Chiba N (2007) On the uniqueness of measuring elastoplastic properties from indentation: the indistinguishable mystical materials. J Mech Phys Solids 55:1618–1660. doi:10.1016/j.jmps.2007.01.010.